

RESPONSE OF SURFACE ACOUSTIC WAVE IMAGING SYSTEMS TO CYLINDRICAL INHOMOGENEITIES

Nilgün Günalp, Bülent Baygün, Fahri Sürücü † and Abdullah Atalar ‡

Middle East Technical University, Ankara, TURKEY

† University of Illinois at Urbana-Champaign, Il., U.S.A.

‡ Bilkent University, Ankara TURKEY

Abstract

Characterization of near-surface properties of materials by acoustic means is most conveniently done by surface acoustic waves (SAW). A conventional acoustic microscope lens excites focused SAW on the object surface, but with a low efficiency. SAW can be excited with a high efficiency and be focused to a diffraction limited spot using conical wavefronts as obtained from a conical axicon. The purpose of this paper is to present the response of the imaging systems utilizing convergent SAW to certain kind of defects. In particular, circular cylindrical cavities, whose axes are perpendicular to surface, are considered. The scattering of the SAW is formulated with some approximations. SAW incident upon the cavity is initially found as an angular spectrum of plane waves. To apply the boundary conditions, the incident field has to be transformed in a form of superposition of cylindrical waves. Similarly, the scattered field, which is found in the form of outgoing cylindrical SAW's, is converted back to a plane wave spectrum to complete the formulation. At the end, a formula is obtained for the output voltage in terms of the position and the radius of the cylinder. By considering various locations for the cylinder, the sensitivity of the system around the focal point is studied. Also, by comparing the output voltages for cylinders of different radii, sensitivity of the system to the size of the inhomogeneity is examined. The numerical results are found to be in agreement with the experimental observations.

I. INTRODUCTION

Surface acoustic waves (SAW) are frequently used for near surface evaluation of materials, because they are very sensitive to surface inhomogeneities like surface breaking cracks [1]. If the characterization is of primary concern rather than just detection of faults, an imaging system may be utilized. The scanning acoustic microscope has been used successfully, because of its ability to excite surface waves [2,3]. The disadvantage of scanning acoustic microscope is that all such modes are excited simultaneously and each with a low efficiency. The efficiency can be increased by use of other configurations. Recently, Köymen and Atalar introduced a method of focusing SAW's on the surface of non-piezoelectric materials by using a new type of conical axicon [4]. Ayter [5] achieved the same, using a conical transducer.

The purpose of this paper is to present a theoretical study of the imaging systems utilizing focused leaky SAW, and their response to certain kind of defects. In particular, circular cylindrical inhomogeneities with perpendicular axes to surface are considered. The surface wave incident upon the inhomogeneity is initially found as an angular spectrum of plane waves. Then, the angular spectrum is converted into a cylindrical wave expansion. At the end, a formula is obtained for the transducer output voltage in terms of the position and the radius of the cylinder, and it is suitable for computer evaluation. By considering various locations for the cylinder, the sensitivity of the system around the focal point is studied. Also, by comparing the output voltages for

cylinders of different radii, sensitivity of the system to the size of the inhomogeneity is examined.

II. FORMULATION

As a representative of SAW imaging systems, we consider the conical axicon focusing system. The operation principle of this system can be found elsewhere [4]. Consider the geometry shown in Fig. 1. The (r, s, t) coordinate system will be used to represent the bulk waves transmitted and received by the transducer, and (x, y, z) coordinates will be used for the surface waves in the solid. The origin of the (x, y, z) coordinate system is chosen at the focal point. Inside the solid a circular cylindrical inhomogeneity is considered. This cylinder extends up to the interface and it is centered at (x_0, y_0) with $y_0 > 0$.

The formulation presented below employs two dimensional potentials $u^+(x, y)$ and $u^-(x, y)$ to represent the incident and scattered surface waves. A time dependence of $\exp(-j\omega t)$ is assumed in the formulation.

Surface Wave Field at the Focus

Let the velocity potential associated with the incident bulk wave be represented by $u_b^+(r, s)$ at the $r-s$ plane. The surface wave field along x -axis and propagating in $+y$ direction, $u_f^+(x)$, can be written as [6]

$$u_f^+(x) = \int_{-\infty}^{\infty} \left\{ \int_{-\infty}^{+\infty} u_b^+(r, s) P(r, s) ds \right\} \exp[-j(k_R/f)rx] dr \quad (1)$$

where $k_R = 2\pi/\lambda_R$ is the real part of the leaky Rayleigh wave number, f is the focal length, and $P(r, s)$ is the pupil function due to finite size of the parabolic mirror. $P(r, s)$ is obtained from a projection of the mirror surface onto $r-s$ plane: a rectangle of width $2x_m$ and height $f \cot \theta_R$, where θ_R is the Rayleigh angle. We have

$$P(r, s) = \begin{cases} e^{-\alpha_T(f-s \tan \theta_R)} e^{jk_R s \cot \theta_R} & \text{for } -x_m < r < x_m \\ & \text{and } 0 < s < f \cot \theta_R \\ 0 & \text{otherwise} \end{cases} \quad (2)$$

where $\alpha_T = \alpha_D + \alpha_L$; α_D and α_L are the dissipation and leak rates, respectively, of the surface wave.

As the incident wave, we assume a unity amplitude uniform plane wave with no r -dependence. The field distribution at $r-s$ plane can be expressed as $u_b^+(r, s) = \exp[-jk_R s \cot \theta_R]$. Using this distribution along with Eq. 2 in Eq. 1 results in the following focal field distribution:

$$u_f^+(x) = \frac{2[1 - \exp(-\alpha_T f)] x_m \cot \theta_R}{\alpha_T} \frac{\sin[(x_m/f)k_R x]}{(x_m/f)k_R x} \quad (3)$$

Field Incident Upon the Cylinder:

By using the angular spectrum approach, the field in the region $y > 0$ can be completely determined by the field distribution at $y = 0$. We

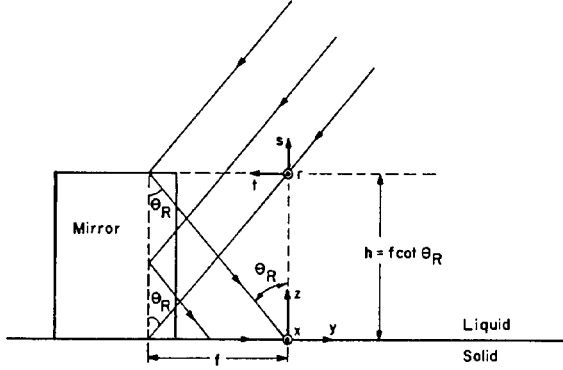


Figure 1: Description of the coordinates used in the formulation.

first define the angular spectrum, $U_f^+(k_x)$, of $u_f^+(x)$ by

$$U_f^+(k_x) = \mathcal{F}\{u_f^+(x)\} = \int_{-\infty}^{+\infty} u_f^+(x) \exp(-jk_x x) dx \quad (4)$$

where \mathcal{F} is the Fourier Transform operator. Then, the angular spectrum at a position $y > 0$ can be written as $U^+(k_x, y) = U_f^+(k_x) \exp(jk_y y)$. The field $u^+(x, y)$ for $y > 0$ can then be written as

$$u^+(x, y) = 1/(2\pi) \int_{-\infty}^{+\infty} U^+(k_x, y) \exp(jk_x x) dk_x, \quad y \geq 0 \quad (5)$$

k_x and k_y are related by $k_x^2 + k_y^2 = k^2$, where k is the complex wave number $k = k_R + j\alpha_T$. We can express k_y as $k_y = (k^2 - k_x^2)^{1/2}$ with $\text{Im}\{k_y\} > 0$. For the assumed plane wave incidence and the pupil function of Eq. 2 we find the angular spectrum of surface waves at $y = 0$ as

$$U_f^+(k_x) = \begin{cases} f\lambda_R[1 - \exp(-\alpha_T f)]/(\alpha_T \tan \theta_R) & |k_x| \leq x_m k_R/f \\ 0 & \text{otherwise} \end{cases} \quad (6)$$

Field Scattered by the Cylinder

To formulate the scattering, we first introduce a primed coordinate system (x', y') with the origin at the center of the cylinder, i.e. $x' = x - x_0$, $y' = y - y_0$ as shown in Fig. 2. To simplify the notation, we also introduce the vectors $\mathbf{r} = (x, y)$, $\mathbf{r}' = (x', y')$, $\mathbf{r}_0 = (x_0, y_0)$, $\mathbf{k} = (k_x, k_y)$. Then, the field incident upon the cylinder can be written as

$$u^+(\mathbf{r}') = 1/(2\pi) \int_{-\infty}^{+\infty} A(k_x) \exp(j\mathbf{k} \cdot \mathbf{r}') dk_x, \quad y' \geq -y_0 \quad (7)$$

where

$$A(k_x) = U_f^+(k_x) \exp(j\mathbf{k} \cdot \mathbf{r}_0) \quad (8)$$

Let $u^-(\mathbf{r}')$ denote the field scattered by the cylinder. Then, the total field outside the cylinder can be written as $u(\mathbf{r}') = u^+(\mathbf{r}') + u^-(\mathbf{r}')$. In order to relate the incident and the reflected fields by the boundary conditions on a cylindrical surface $\rho' = a$, it is necessary to express these fields in terms of cylindrical wave functions. The incident field which will be evaluated at $\rho' = a$ can be expressed in terms of regular cylindrical wave functions as

$$u^+(\mathbf{r}') = \sum_{n=-\infty}^{+\infty} K_n \exp(jn\phi') J_n(k\rho') \quad (9)$$

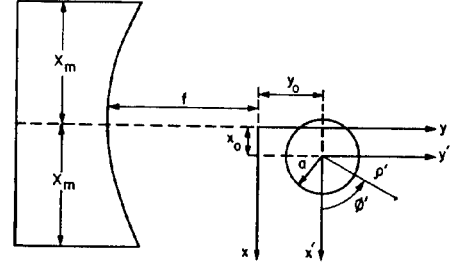


Figure 2: Top view depicting the primed coordinate system.

and the scattered field can be expanded in terms of outgoing cylindrical wave functions as

$$u^-(\mathbf{r}') = \sum_{n=-\infty}^{+\infty} B_n \exp(jn\phi') H_n^{(1)}(k\rho'), \quad \rho' \geq a \quad (10)$$

The relationship between $\{K_n\}$ of Eq. 9 and $A(k_x)$ of Eq. 7 can be established by substituting the following transformation formula [7] into Eq. 7

$$\exp(j\mathbf{k} \cdot \mathbf{r}') = \sum_{n=-\infty}^{+\infty} \exp(jn\pi/2) \exp(jn\phi') J_n(k\rho') \left(\frac{k_x - jk_y}{k}\right)^n$$

This yields

$$K_n = 1/(2\pi) \exp(jn\pi/2) \int_{-\infty}^{+\infty} A(k_x) \left(\frac{k_x - jk_y}{k}\right)^n dk_x \quad (11)$$

The next step in the formulation is to express $\{B_n\}$, the expansion coefficients of the scattered wave, in terms of $\{K_n\}$. Although only the scattered surface wave, will induce an output voltage at the transducer, for an exact solution of the problem all possible field components should be taken into account. Such an exact formulation is quite complicated [8], therefore a simple approximate method will be applied: Since the finite value of c_{44} makes the surface of the cylinder a relatively hard boundary in the radial direction, the total surface wave along the interface will be forced to satisfy the rigid-boundary condition ($v_{\rho'} = 0$ at $\rho' = a$). Use of the free-boundary condition is not appropriate here, it approximates a cavity in a liquid medium where c_{44} is zero. Even though the inhomogeneity is a cavity, it is better approximated in the scalar approximation by a rigid cylinder. This approximate formulation does not give the actual "ratio" of the scattered surface wave to the incident. However, it can quite satisfactorily be used to compare the scattered fields due to various cylinders of different locations and sizes. When the boundary condition $\partial/\partial\rho'\{u^+(\mathbf{r}') + u^-(\mathbf{r}')\}|_{\rho'=a} = 0$ is applied with $u^+(\mathbf{r}')$ and $u^-(\mathbf{r}')$ as given by Eqns. 9 and 10, one obtains

$$B_n = T_n K_n \quad (12)$$

where

$$T_n = -j_n(ka)/\dot{H}_n^{(1)}(ka) \quad (13)$$

The scattered surface wave, which was expressed in cylindrical form in Eq. 10, must now be written as

$$u^-(x, y) = 1/(2\pi) \int_{-\infty}^{+\infty} U_f^-(k_x) \exp[j(k_x x - jk_y y)] dk_x \quad (14)$$

for points $y \leq y_0$. Note that $U_f^-(k_x)$ corresponds to the returning angular spectrum at $y = 0$. Using the transformation formula [7]

$$e^{jn\phi'} H_n^{(1)}(k\rho') = \frac{e^{-jn\pi/2}}{\pi} \int_{-\infty}^{+\infty} \left(\frac{k_x - jk_y}{k}\right)^n e^{j(k_x x' - k_y y')} / k_y dk_x \quad (15)$$

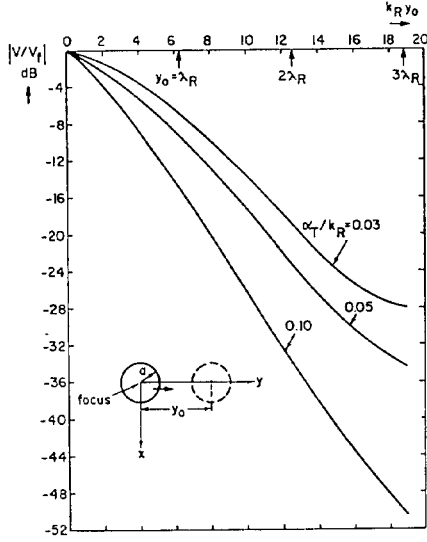


Figure 3: Normalized transducer output voltage as a function of the axial position of the cylinder for several α_T/k_R values. ($x_m/f = 0.74$, $k_R a = 0.5$, $x_0 = 0.0$, $V_f =$ output voltage when the cylinder is centered at the focus. V_f is 12.73 dB below V_{edge})

for $y' \leq 0$ in Eq. 10, one can recognize $U_j^-(k_x)$ of Eq. 14 to be

$$U_j^-(k_x) = \sum_{n=-\infty}^{+\infty} 2B_n \frac{\exp(-jn\pi/2)}{k_y} \left(\frac{k_x - jk_y}{k}\right)^n \exp[-j(k_x x_0 - k_y y_0)] \quad (16)$$

Transducer Output Voltage:

The scattered surface wave $u^-(x, y)$ travels in backward direction and leaks into the liquid. This leak field gets collimated in the transducer direction after being reflected from the mirror. The field incident upon the transducer, $u_b^-(r, s)$, can be obtained by [6]

$$u_b^-(r, s) = \alpha_L P(r, s) \int_{-\infty}^{+\infty} u_j^-(x) \exp(-j\frac{k_R}{f} r x) dx \quad (17)$$

where $u_j^-(x) = u^-(x, 0)$ is the scattered surface wave field along the x-axis. Eq. 17, when combined with the fact that $U_j^-(k_x) = \mathcal{F}\{u_j^-(x)\}$ as in Eq. 4, yields

$$u_b^-(r, s) = \alpha_L P(r, s) U_j^-\left(\frac{k_R}{f} r\right) \quad (18)$$

Finally, since $u_b^-(r, s)$ is to be received by the same transducer generating the incident field, $u_b^+(r, s)$, the output voltage of the transducer can be expressed as

$$V = \int_{-\infty}^{+\infty} \int_{-\infty}^{+\infty} u_b^+(r, s) u_b^-(r, s) dr ds$$

By the substitution of Eqs. 2 and 18, this expression simplifies to

$$V = \frac{\alpha_L}{\alpha_T \tan \theta_R} [1 - \exp(-\alpha_T f)] \int_{-x_m}^{+x_m} U_j^-\left(\frac{k_R}{f} r\right) dr \quad (19)$$

Then, $U_j^-\left[\left(\frac{k_R}{f} r\right)\right]$ is evaluated by combining Eqs. 16, 12, 11, 8 and 6, and the final form of Eq. 19 is obtained as

$$V = \frac{V_{edge}}{2\pi k_R (x_m/f)} \sum_{n=-\infty}^{+\infty} T_n P_n(\mathbf{r}_0) Q_n(\mathbf{r}_0) \quad (20)$$

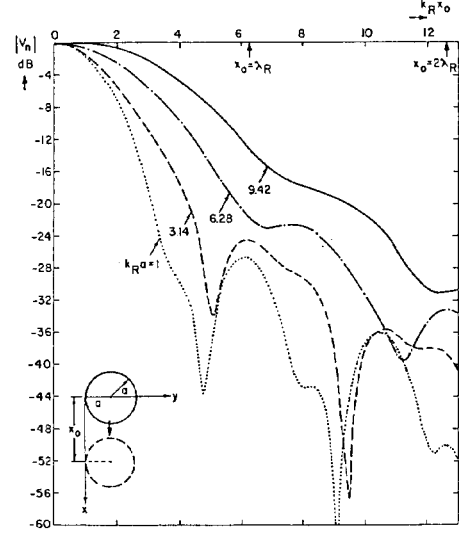


Figure 4: Normalized transducer output voltage as a function of the lateral position of the cylinder with the cylinder radius as the parameter.

where

$$P_n(\mathbf{r}_0) = \int_{-(x_m/f)k_R}^{(x_m/f)k_R} \exp[j(k_x x_0 + k_y y_0)] \left(\frac{k_x - jk_y}{k}\right)^n dk_x \quad (21)$$

$$Q_n(\mathbf{r}_0) = \int_{-(x_m/f)k_R}^{(x_m/f)k_R} \exp[-j(k_x x_0 - k_y y_0)] \left(\frac{k_x - jk_y}{k}\right)^n dk_x / k_y \quad (22)$$

$k_y = (k^2 - k_x^2)^{1/2}$, $k = k_R + j\alpha_T$, and T_n is as given by Eq. 13. V_{edge} corresponds to the transducer output voltage when there is an infinitely long edge (plane reflector) along the x-axis. To find it we assume that $U_j^-(k_x) = U_j^+(k_x)$ which means a total reflection. In this case Eq. 19 yields

$$V_{edge} = 2x_m \alpha_L \lambda_R f \left(\frac{1 - \exp(-\alpha_T f)}{\alpha_T \tan \theta_R}\right)^2$$

This expression shows the factors effecting the output voltage with a perfect SAW reflector at the focal line.

III. NUMERICAL RESULTS

Eq. 20 gives the transducer output voltage in terms of the center, $\mathbf{r}_0 = (x_0, y_0)$, and the radius, a , of the scattering cylinder. The integrals P_n and Q_n given by Eqs. 21 and 22 depend only on the position of the cylinder, whereas the coefficient T_n depends only on the radius. Hence, these integrals, once evaluated at a certain (x_0, y_0) position, can be stored and be used subsequently for cylinders of different radii centered at the same point. We put the integrals P_n and Q_n into a form more suitable for numerical integration by using a simple change of variables: $p = k_x / [(x_m/f)k_R]$. For the calculation of V/V_{edge} , the only parameters that must be specified are x_m/f , α_T/k_R , $k_R x_0$, $k_R y_0$ and $k_R a$. The necessary number of integration points increases as n and/or the distance of the center from focal point increases. For the calculation of T_n , the derivatives of the Bessel and Hankel functions of the complex argument $ka = k_R a(1 + j\alpha_T/k_R)$ are generated. For small cylinders with $k_R a < 1$ only the terms with $|n| \leq 3$ in the summation of Eq. 20 are sufficient. As the radius increases, more and more terms should be included.

In order to compare our results with the previously published experimental results [9], we chose $x_m/f = 0.74$ in all of the calculations given below. The ratio α_T/k_R is equal to 0.03 for aluminum, and this value

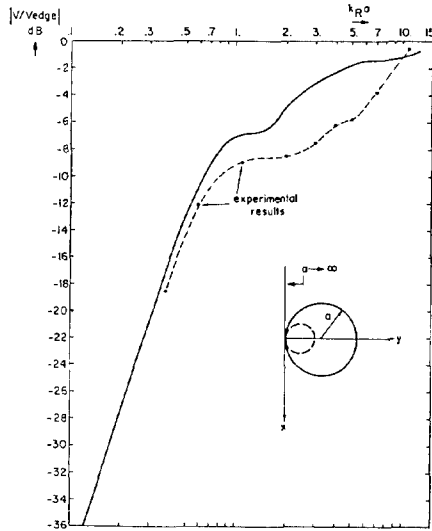


Figure 5: Variation of the output voltage with the cylinder radius. ($x_m/f = 0.74$, $\alpha_T/k_R = 0.03$, $x_0 = 0.0$, $y_0 = a$, V_{edge} : output voltage corresponding to the case $a \rightarrow \infty$).

is used in all of the presented results, except in Fig. 3, where several α_T/k_R ratios are considered.

The first set of results given in Fig. 3 corresponds to a small cylinder ($k_R a = 0.5$, diameter $\approx 0.16\lambda_R$) moved along the y -axis to see the axial sensitivity of the imaging system. Here the results are normalized by the transducer output voltage, V_f , obtained when the cylinder is centered at the focus. Curves corresponding to different α_T/k_R ratios are presented. In each case it is seen that as the scatterer moves away from the focal point, the output voltage decreases monotonically. For the case of $\alpha_T/k_R = 0.03$ (A), 20 dB drop at the output voltage occurs at $k_R y_0 = 13$ which corresponds to a distance $y_0 \approx 2\lambda_R$ from the focal point. This result is in close agreement with our experimental observations. It is interesting to note that as the leak rate is increased the response of the system in y direction gets sharper, i.e. the resolution in y direction increases.

To examine the sensitivity of the system along x -direction (lateral direction), several calculations are carried out. Fig. 4 shows how the output voltage varies in the lateral direction. Here, the cylinders of different radii are moved parallel to the x -axis (with their edges touching the x -axis), and the corresponding output voltages are plotted after being normalized by their maximum values. It is seen that for cylinders whose diameters are larger than the width of the main beam of the incident sinc function, the transducer output voltage is related rather closely to the size of the cylinder. For $k_R a = 2\pi$ and $k_R a = 3\pi$, approximately 20 dB drop in the output voltage is obtained when the cylinder is centered at the position $x_0 = a$. Hence images obtained in such a system will correctly depict the size of the cylinders. But, for small cylinders, the response of the system is determined by the incident sinc function. It is also observed that the resolution of the system in x direction is about 4 times better than in y direction for the case of aluminum sample, and this is consistent with experimental results.

Finally, to investigate the sensitivity of the imaging system to the radius of the cylinder, the output voltages for different radii are calculated. Each cylinder is centered at the point $x_0 = 0$, $y_0 = a$, where a is its radius, so that the edge of each cylinder is at the focus as demonstrated in Fig. 5. The case $a \rightarrow \infty$ corresponds to an infinite straight edge reflector along x -axis for which the transducer output voltage is V_{edge} . All voltages are normalized by V_{edge} and plotted vs $k_R a$. It is observed that the output voltage increases as the cylinder becomes larger, and for $k_R a = 3.1$ ($a \approx \lambda_R/2$), the output voltage is only 3 dB below V_{edge} . This is because the incident field $u_f^+(x)$ illuminates only a finite portion

along x -axis. Thus, increasing the radius further will not change the output voltage considerably. On the other hand, for small radii the signal drops about 10 dB for halving the the cylinder radius. The asymptotic line crosses the 0 dB axis at around $k_R a = 1$.

The curve in Fig. 5 exhibits another interesting feature. As $k_R a$ approaches 1 from smaller values, the output voltage tends to increase faster, thus forming a local maximum at $k_R a = 1$. This corresponds to a cylinder whose circumference is λ_R , i.e. the phase change around the cylinder is 2π . Such behaviour can be explained by the in-phase superposition of the creeping surface waves around the cylinder. The dots in the figure represent the experimental results obtained earlier [9]. Although in the experimental setup, the focal field had a wider beamwidth, the experimental curve possesses the same kind of signal enhancement around $k_R a = 1$.

IV. CONCLUSIONS

We have presented a theory to predict the response of a SAW imaging system. In particular, we calculated the response to cylindrical cavities as a function of position of cavity with respect to focus point. The calculations indicated that the leak rate affects the resolution of the system in the y -direction. A high leak rate material will result in a better resolution in y -direction. The theory also predicts an enhancement in the received signal level when the cylinder circumference equals a SAW wavelength. The images of cylinders obtained with such systems will indicate the size of the cylinders correctly at 20 dB below its peak value as long as the cylinder diameter is larger than about a Rayleigh wavelength. For small cylinders the received peak amplitude can be used to determine the size of the cylinder.

References

- [1] R.J. Dewhurst, A.D.W. McKie, and S.B. Palmer, "Further evidence for two-component surface acoustic wave reflections from surface breaking cracks," *Appl. Phys. Lett.*, vol. 49, pp. 1694-1695, 1986.
- [2] K. Yamanaka, Y. Enomoto and Y. Tsuya, "Acoustic microscopy of ceramic surfaces," *IEEE Trans. Son. Ultrason.*, vol. 32, pp. 313-319, 1985.
- [3] G.C. Smith, M.G. Gee, "Observation of a sub-surface defect in sapphire by Rayleigh wave reflection in the scanning acoustic microscope," *J. Mater. Sci. Lett.*, vol. 5, pp. 1133-1134, 1986.
- [4] H.Köymen, and A. Atalar, "Focusing surface waves using an axicon," *Appl. Phys. Lett.*, vol. 47, pp. 1266-1268, 1985.
- [5] S. Ayter, "Focusing surface waves using conical transducers," in *Proc. of 1987 IEEE Ultrason. Symp.*, pp. 301-304, 1987.
- [6] A. Atalar, and H. Köymen, "V(Z) of the surface acoustic wave focusing system," in *IEEE 1986 Ultrasonics Symposium Proceedings*, pp. 727-730, 1986.
- [7] N. Günalp, "Acoustic and electromagnetic scattering from cylinders buried in a half space," Ph.D. Thesis, Middle East Tech. Univ., 1981.
- [8] A. Gantesen, "Scattering of an obliquely incident Rayleigh wave in an elastic quarterspace," *Wave Motion*, vol. 8, pp. 27-41, 1986.
- [9] A. Atalar, and H. Köymen, "Use of a conical axicon as a surface acoustic wave focusing device," *IEEE Trans. Ultrason. Ferroelect. Freq. Contr.*, vol. 34, pp. 53-63, 1987.